CHAPTER 6

VALIDATION OF SOLAR WATER HEATER SYSTEM AND ECONOMICS ANALYSIS

In this chapter, validations of the mathematical models of evacuated tube solar water heater system are performed with the experiment results. The solar water heater system consists of 8 evacuated tubes and volume of the water storage tank is 100 liters. The solar water heater system is tilted at 18.8^{o} from horizontal and facing to south. The radiation shield covering the solar collector is removed at 08:00 a.m. and the experiments is carried out from 8:00 a.m. to 4:00 p.m. during August to October, 2016 on a partly cloudy day and a clear sky day under the climatic conditions of Chiang Mai province, Thailand. In addition, K-type thermocouples, pyranometer, and anemometer are used to measure temperatures, solar intensity, and wind velocity, respectively. After that, the climatic conditions of Chiang Mai are taken as the input data of the mathematical models. The mathematical results, the temperatures, heat rate of water, and thermal efficiency of a partly cloudy day and a clear sky day are validated by the experiment results under the identical climatic conditions of the experiment.

6.1 Validation of evacuated tube solar water heater system models

In order to validate the mathematical models, the different climatic conditions of the experiment are selected for a partly cloudy day and a clear sky day. The solar intensity, ambient air temperature, and average wind velocity are based on Chiang Mai province, Thailand during 8:00 a.m. to 4:00 p.m. on August 18, 2016 which represents climatic condition of a partly cloudy day while October 14, 2016 represents a clear sky condition. Therefore, the weather data is presented in Figure 6.1. This data is inputted to the mathematical models for predicting the temperatures of the solar water heater system.

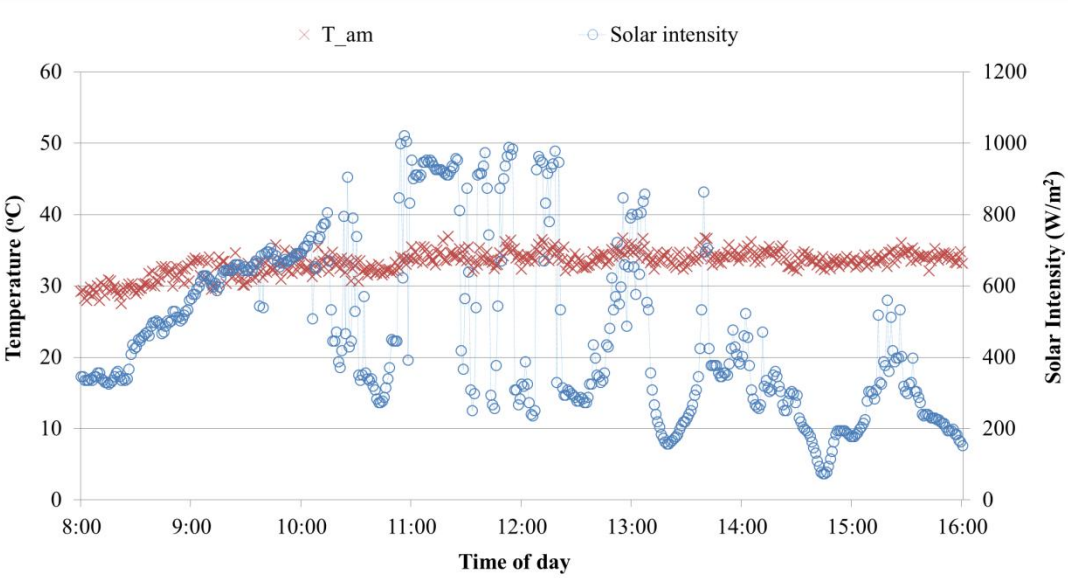

(a) Partly cloudy day condition (August 18, 2016)

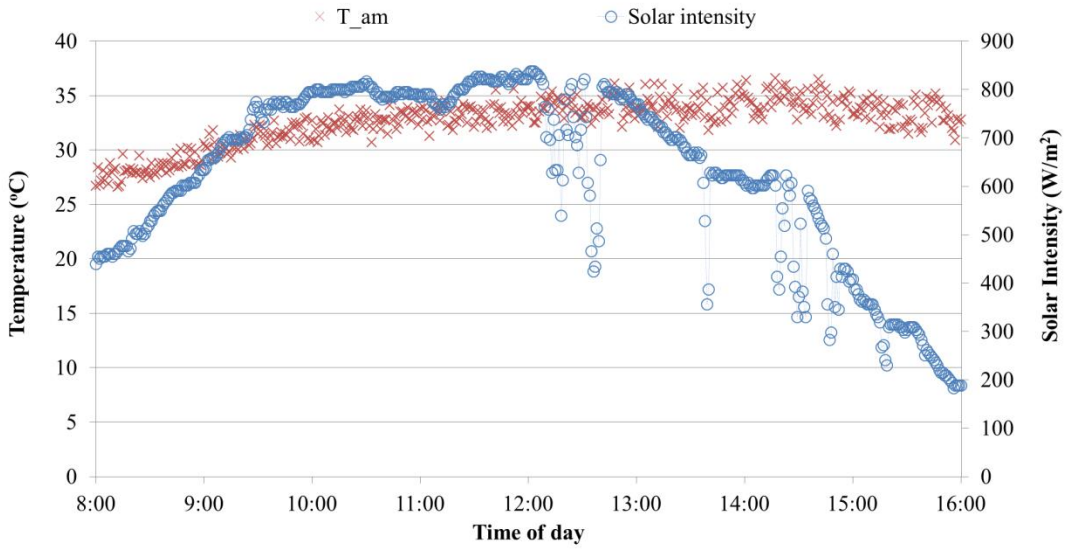

(b) Clear sky day condition (October 14, 2016)

Figure 6.1 Weather data of Chiang Mai province, Thailand

The partly cloudy day and the clear sky day of the mathematical models are validated to the experiment results as shown in Figure 6.2 to Figure 6.18.

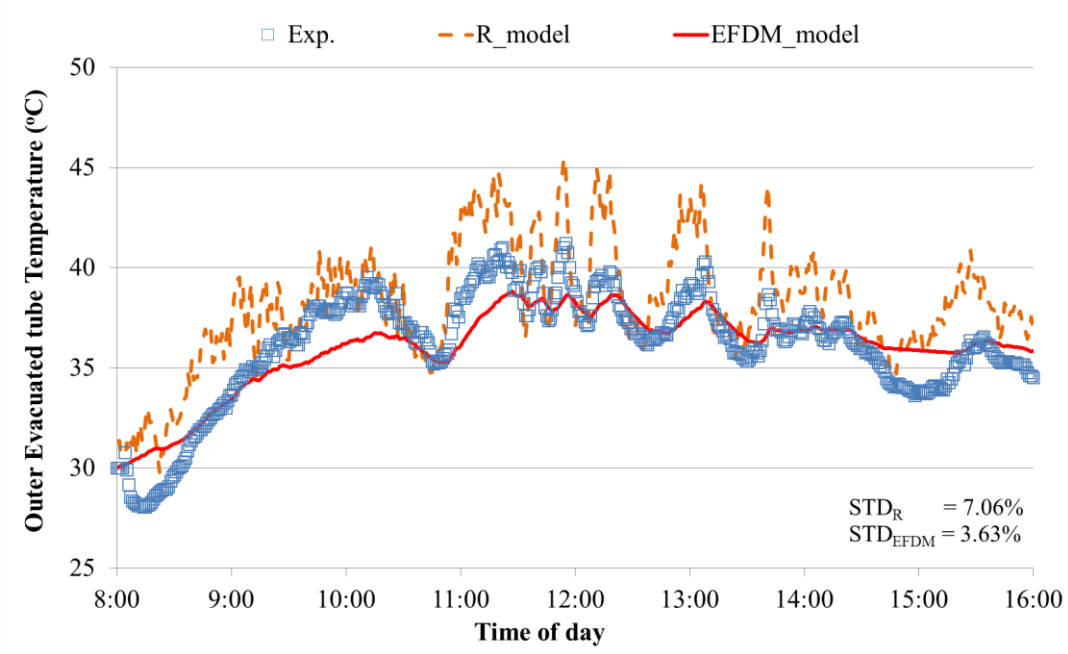

(a) Partly cloudy day condition (August 18, 2016)

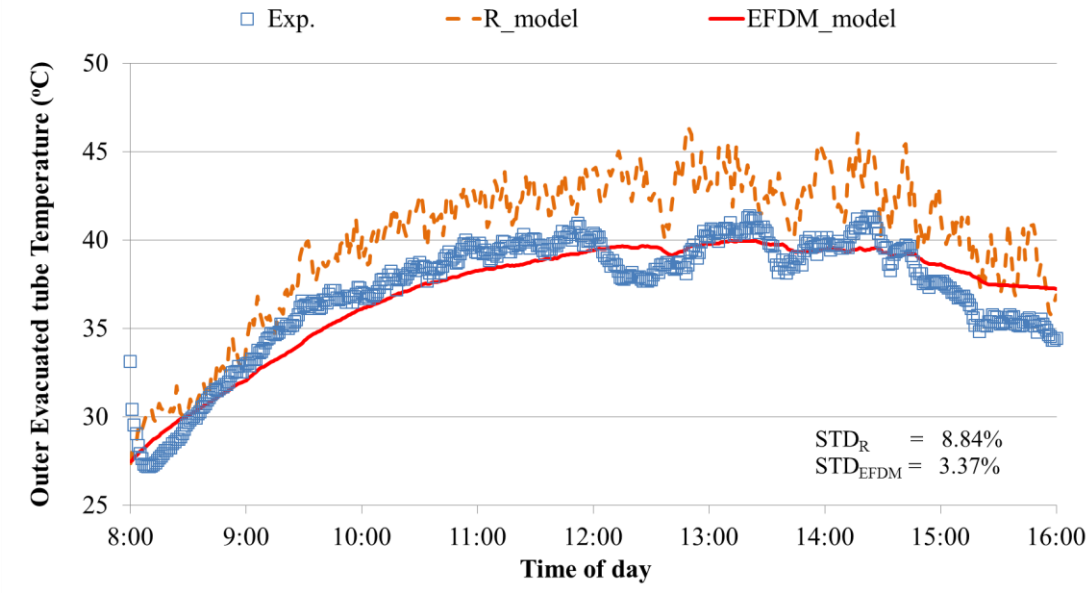

(b) Clear sky day condition (October 14, 2016)

Figure 6.2 Temperatures of the outer evacuated tube along with local time

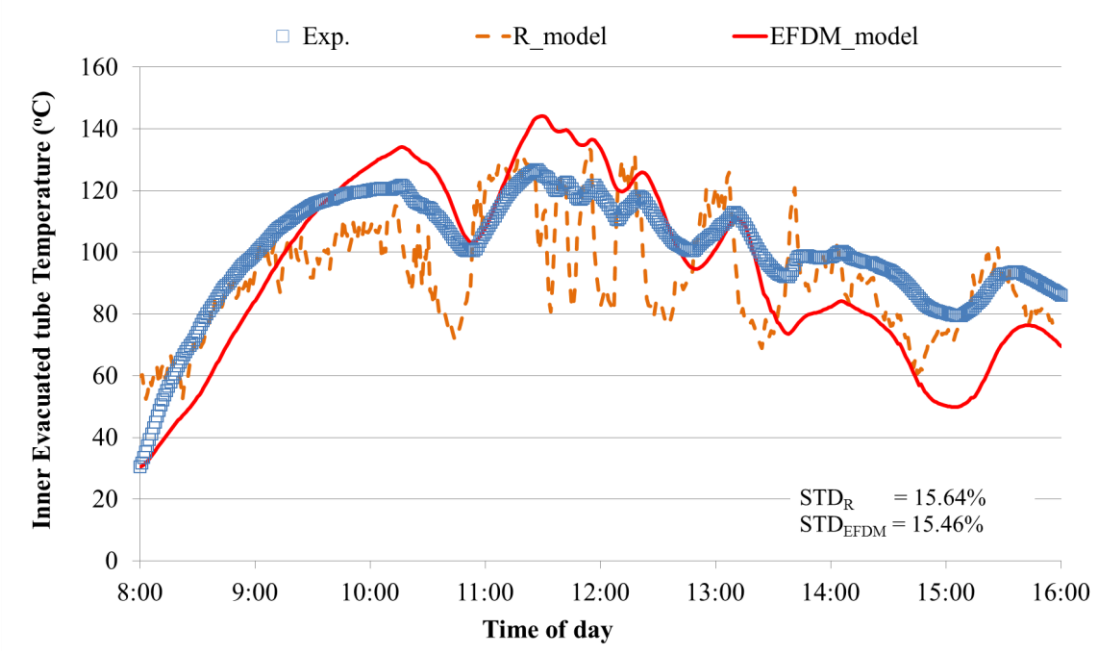

(a) Partly cloudy day condition (August 18, 2016)

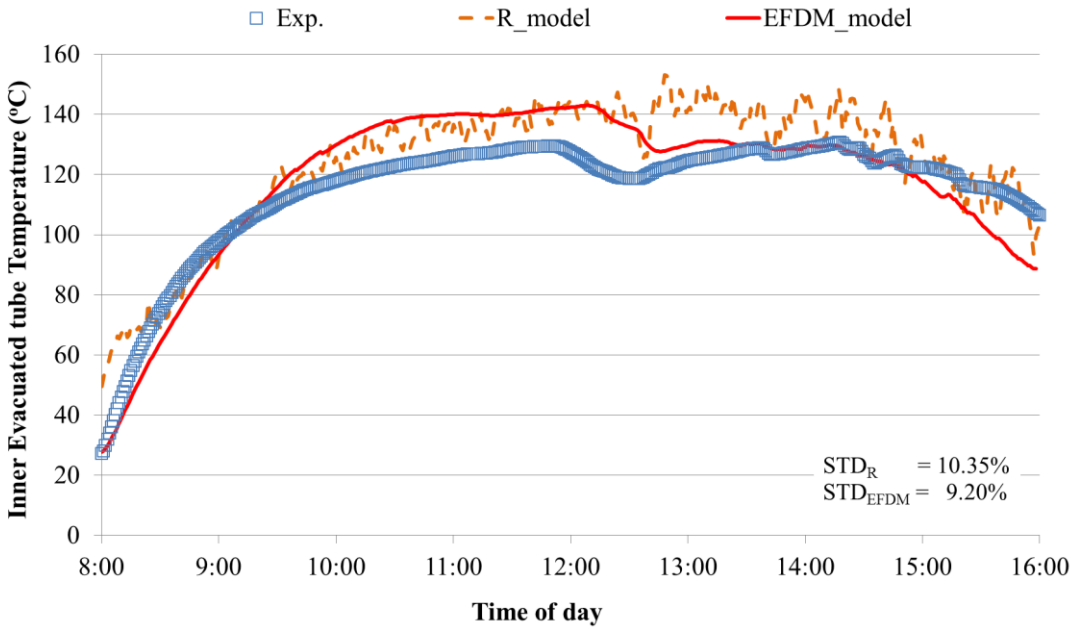

(b) Clear sky day condition (October 14, 2016)

Figure 6.3 Temperatures of the inner evacuated tube along with local time

The outer evacuated tube temperatures of the experiment and both models of a partly cloudy day and a clear sky day are presents in Figure 6.2. It is found that the temperatures of the both models are shown a similar trend with the experiment of partly

cloudy and clear sky conditions. The EFDM result of outer evacuated tube is a good agreement with the experiment results. However, the outer evacuated tube of thermal resistance method is higher than the experiment and EFDM for the both climate conditions. Moreover, the STD of outer evacuated tube temperature for a partly cloudy condition is ±7.06% of the thermal resistance method and ±3.63% of EFDM. For clear sky day condition, the STD is ±8.84% of the thermal resistance method and ±3.37% of EFDM.

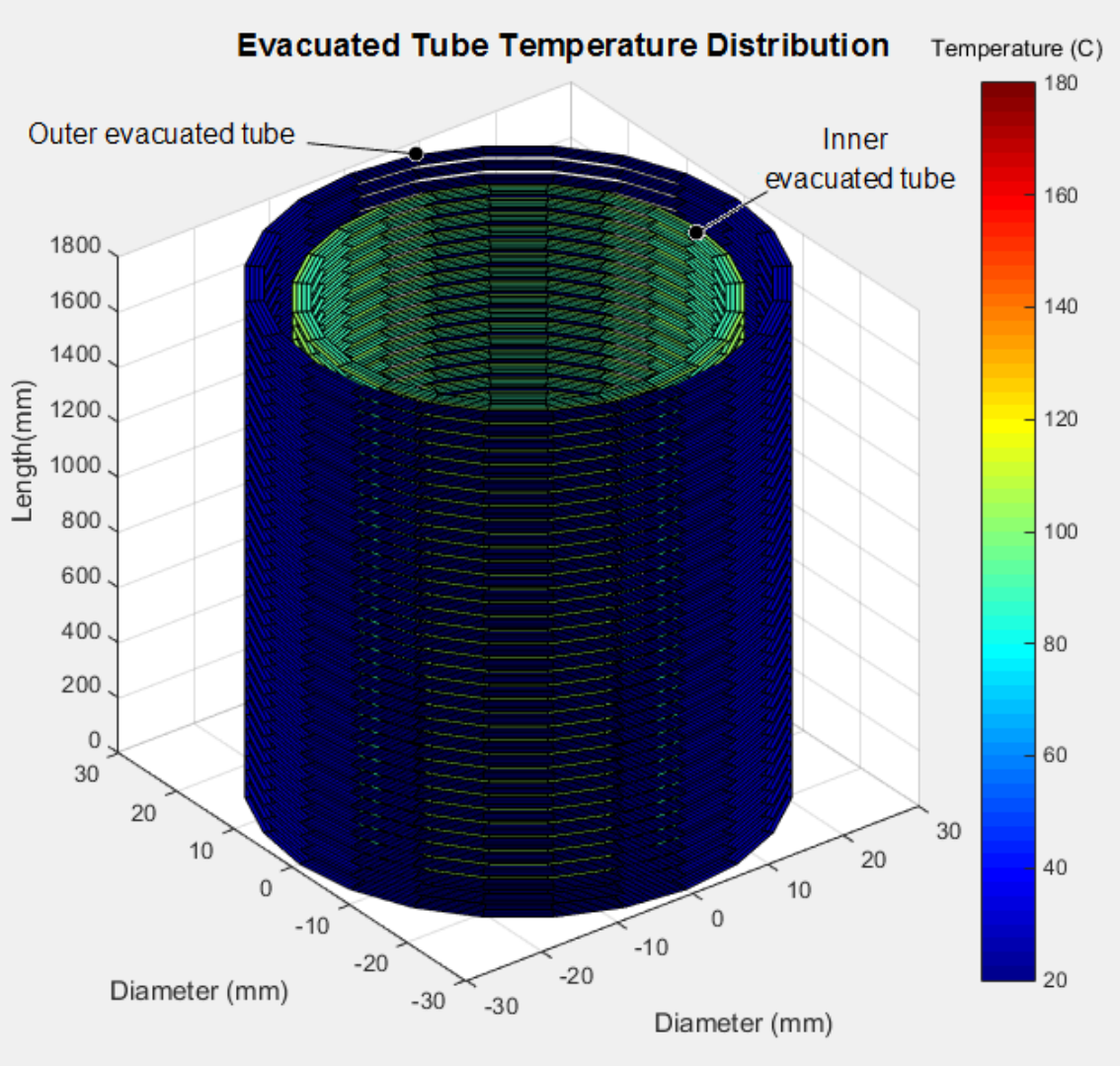

Figure 6.4 Evacuated tube domains

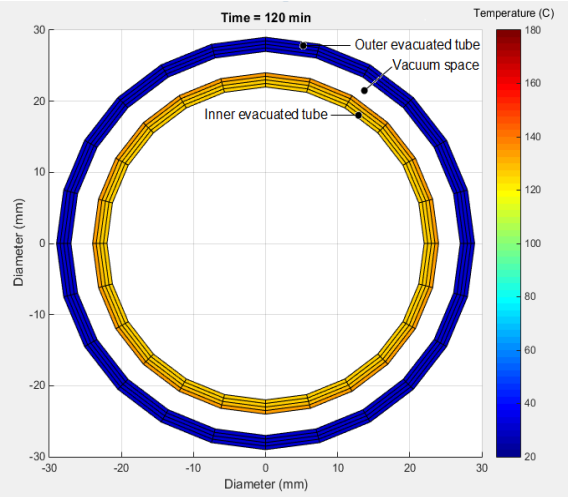

(a) Temperature distribution at 10:00 a.m.

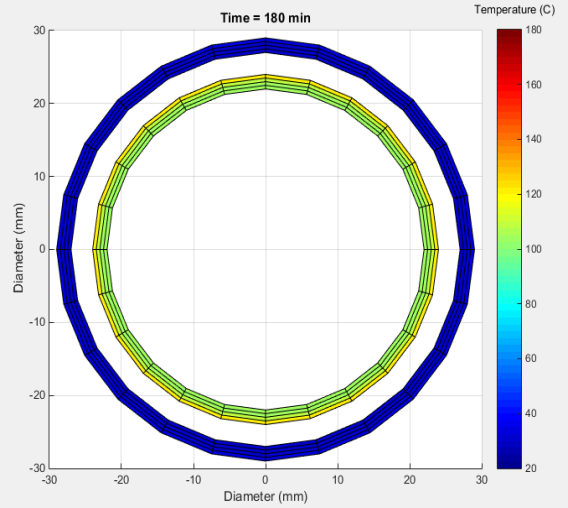

(b) Temperature distribution at 11:00 a.m.

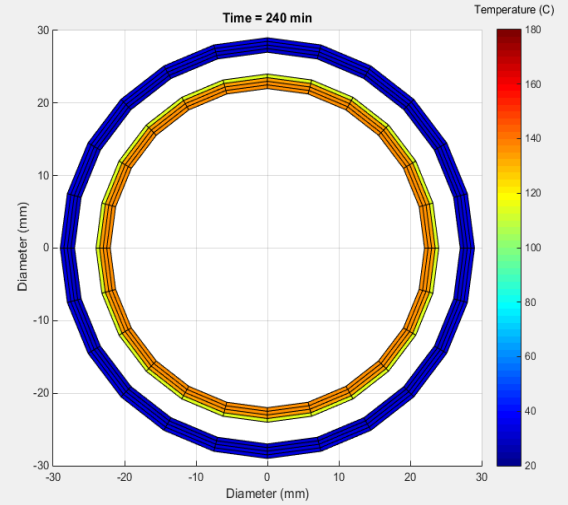

(c) Temperature distribution at 12:00 p.m.

Figure 6.5 Temperature distribution of evacuated tube for partly cloudy day condition on August 18, 2016

Temperature of the inner evacuated tube is shown in Figure 6.3. It can be seen that the temperatures of inner evacuated tube of both models representing different weather conditions are in a similar trend with the experiment. On a partly cloudy day, the STD of the thermal resistance method is ±15.64% and ±15.46% for EFDM. On the contrary, for a clear sky day, the STD of the thermal resistance method is ±10.35% and ±9.20% for EFDM.

The evacuated tube domains of EFDM are shown in Figure 6.4. In order to observe the temperature distribution of evacuated tube, cross-sectional view of evacuated tube is presented as in Figure 6.5 for a partly cloudy day condition on August 18, 2016. From Figure 6.3 (a) and Figure 6.5, it can be noted that the temperature of inner evacuated tube during 9:00 a.m. to 10:00 a.m. is increased. The temperature distribution of evacuated tube in Figure 6.5 (a) shows high temperature. On the other hand, in Figure 6.3, the temperature of inner evacuated tube during 10:00 a.m. to 11:00 a.m. is decreased. The temperature distribution of evacuated tube in Figure 6.5 (b) it is shows that the temperature is lower than the temperature in Figure 6.5 (a). Then, the temperature of inner evacuated tube and the temperature distribution are increased as shown in Figure 6.3 (a) and Figure 6.5 (c), respectively.

The temperature distribution of evacuated tube of clear sky day condition on October 14, 2016 and cross-sectional view of evacuated tube are presented in Figure 6.6. According to Figure 6.3 (b) and Figure 6.6, it can be seen that the temperature has continuously increased during 10:00 a.m. to 12:00 p.m. as shown in Figure 6.3 (b). From the temperature in Figure 6.3 (b), the temperature distribution is presented in Figure 6.6, it is continuously increased which is not fluctuated as same as Figure 6.5 because of the consistently solar intensity.

Temperatures of the evaporator are presented in Figure 6.7. It shows that temperatures of both models are in a similar trend with the experiments. The evaporator temperature of partly cloudy day condition is more fluctuated than the clear sky day condition. Therefore, it will affect to the evaporator temperature of the thermal resistance method to be fluctuated more than EFDM on a partly cloudy day.

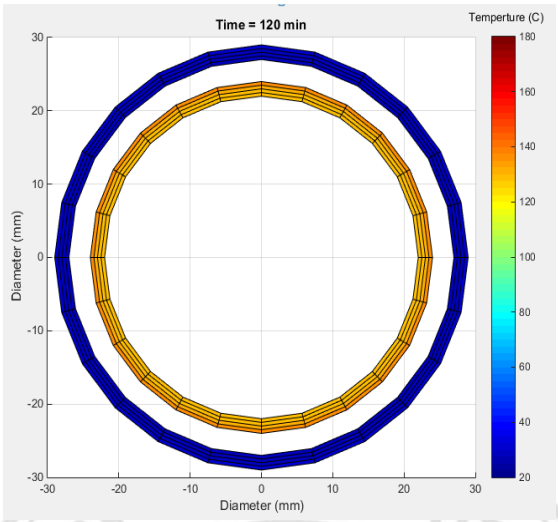

(a) Temperature distribution of evacuated tube at 10:00 a.m.

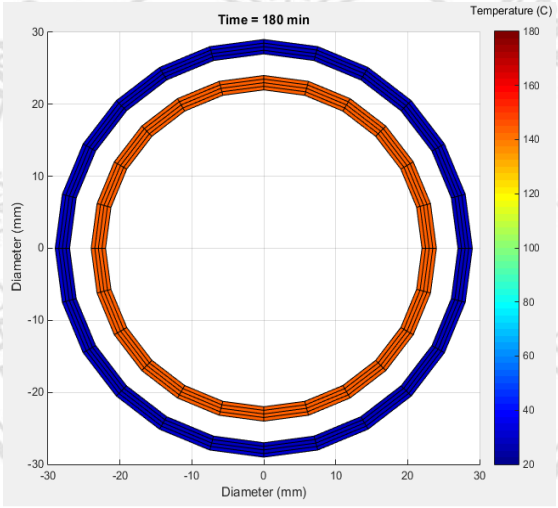

(b) Temperature distribution of evacuated tube at 11:00 a.m.

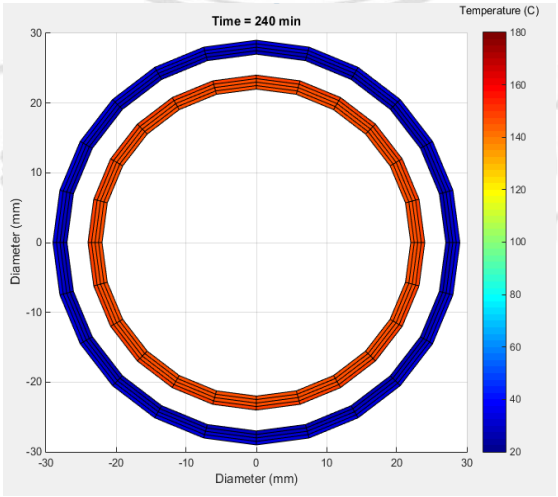

(c) Temperature distribution of evacuated tube at 12:00 p.m.

Figure 6.6 Temperature distribution of evacuated tube for clear sky day condition on October 14, 2016

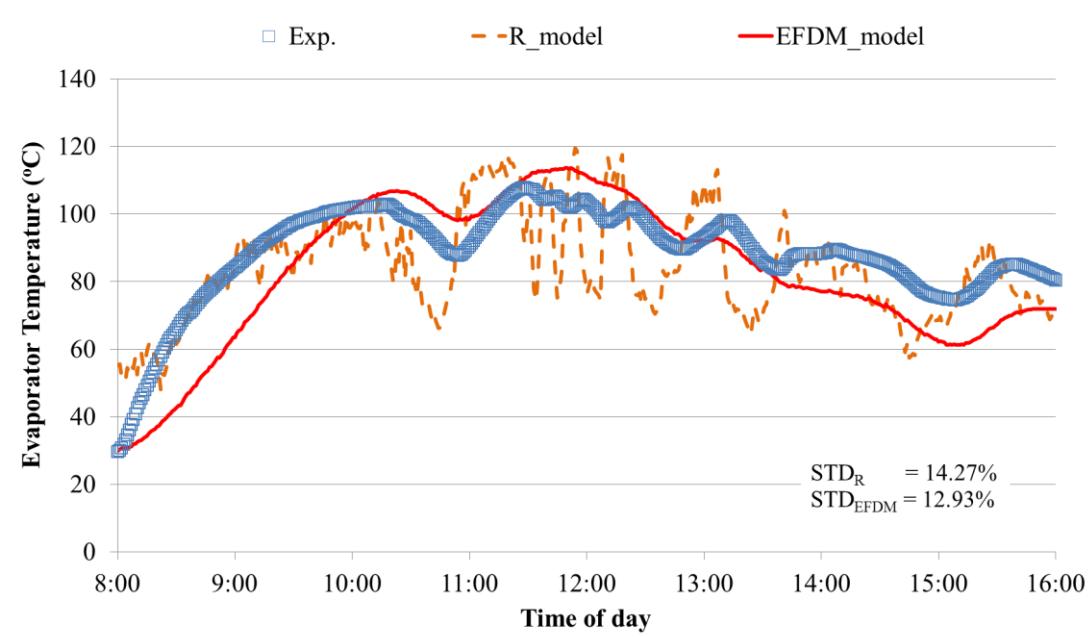

(a) Partly cloudy day condition (August 18, 2016)

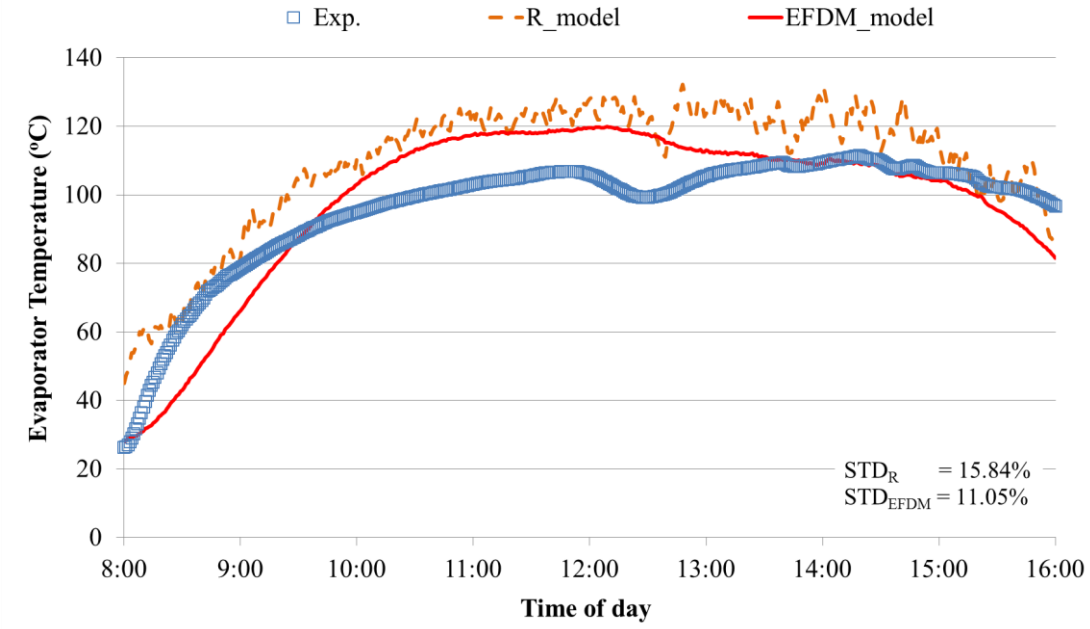

(b) Clear sky day condition (October 14, 2016)

Figure 6.7 Evaporator temperatures along with local time

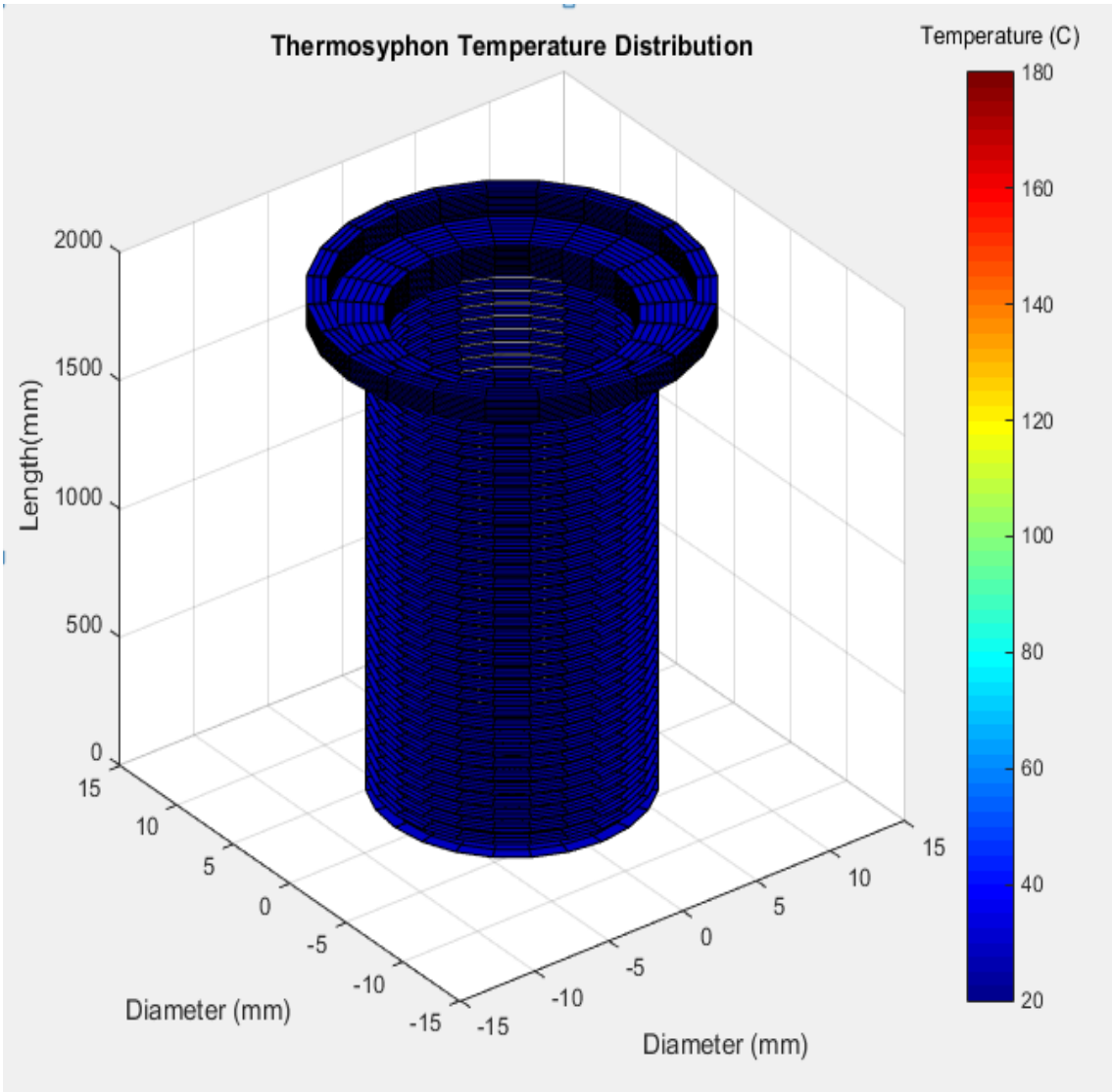

Figure 6.8 Thermosyphon domain

The thermosyphon domain of EFDM is shown in Figure 6.8. The themosyphon diameter of evaporator section and condenser section are 15.88 mm and 22.22 mm, respectively. The thermosyphon temperature distribution of evaporator section is presented in cross-sectional view in Figure 6.9 for partly cloudy day condition on August 18, 2016. From Figure 6.7 (a), it can be noted that the evaporator temperature is increased during 9:00 a.m. to 10:00 a.m. while it is decreased during 10:00 a.m. to 11:00 a.m. due to fluctuated solar intensity of this time period. This is in good agreement with the temperature distribution of evaporator section in Figure 6.9 (a) and (b). Moreover, the evaporator temperature during 11:00 a.m. to 12:00 p.m. is increased and then decreased until 1:00 p.m. because the solar intensity is also fluctuated the same

time as the previous time period, which is during 9:00 a.m. to 11:00 a.m. It can be seen that the temperature distribution in Figure 6.9 (c) and (d) shows good agreement with Figure 6.7 (a) for partly cloudy day condition.

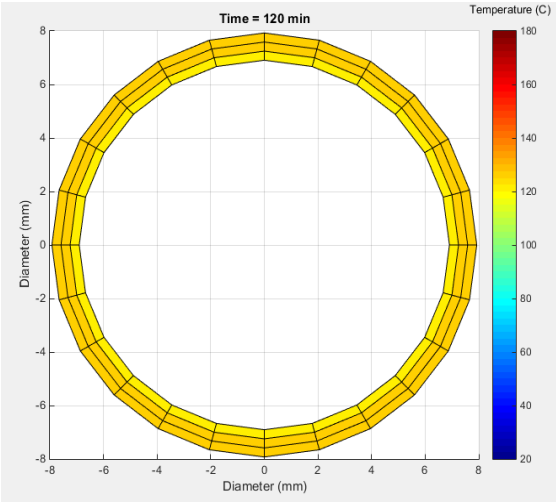

(a) Temperature distribution at 10:00 a.m.

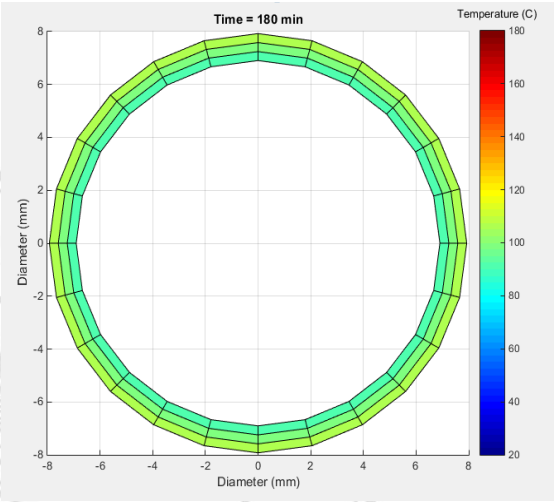

(b) Temperature distribution at 11:00 a.m.

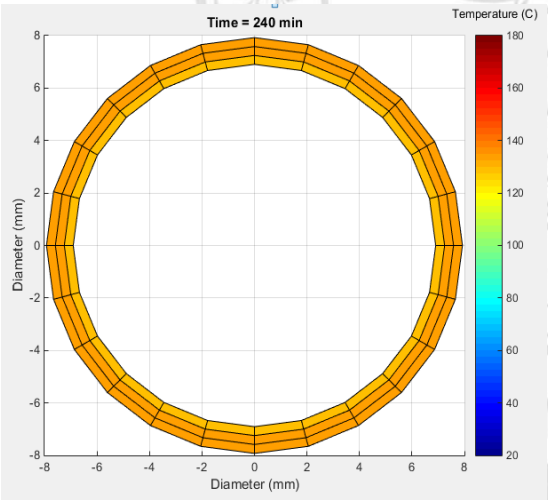

(c) Temperature distribution at 12:00 p.m.

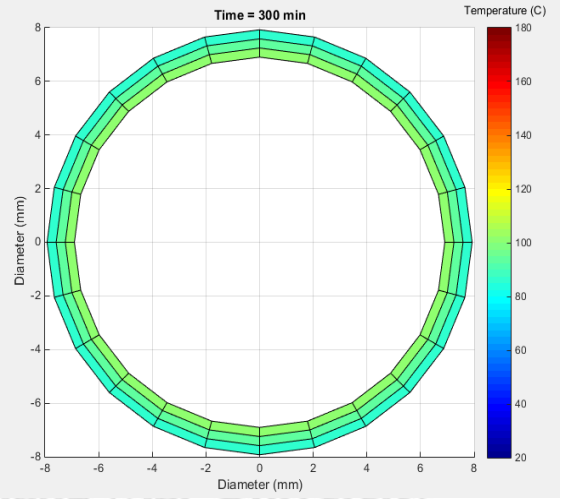

(d) Temperature distribution at 1:00 p.m.

Figure 6.9 Temperature distribution of evaporator section for partly cloudy day condition on August 18, 2016

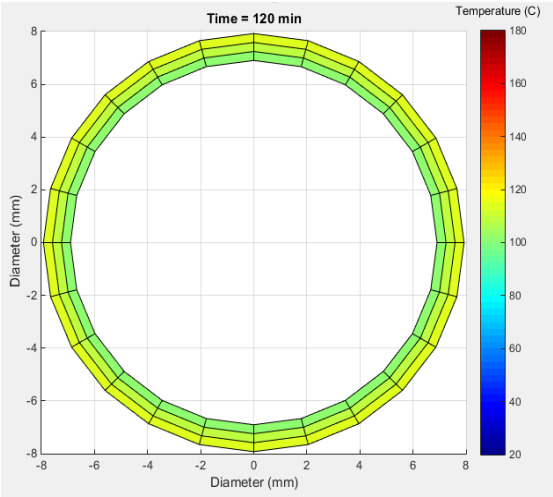

(a) Temperature distribution at 10:00 a.m.

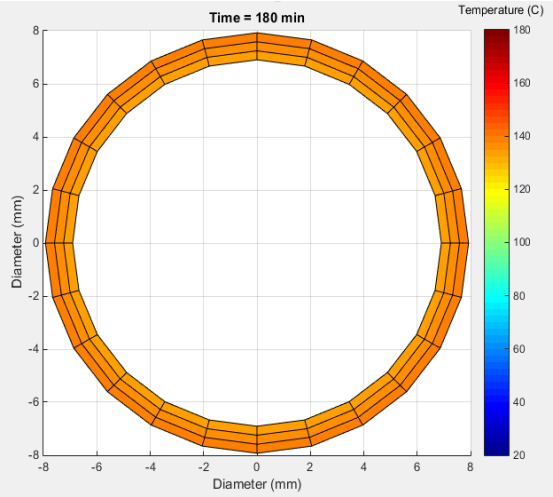

(b) Temperature distribution at 11:00 a.m.

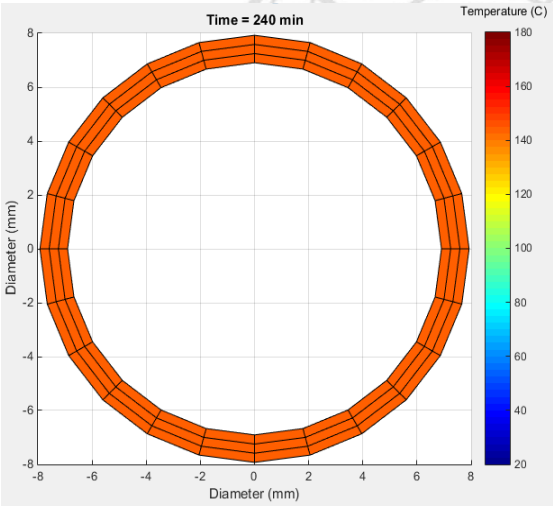

(c) Temperature distribution at 12:00 p.m.

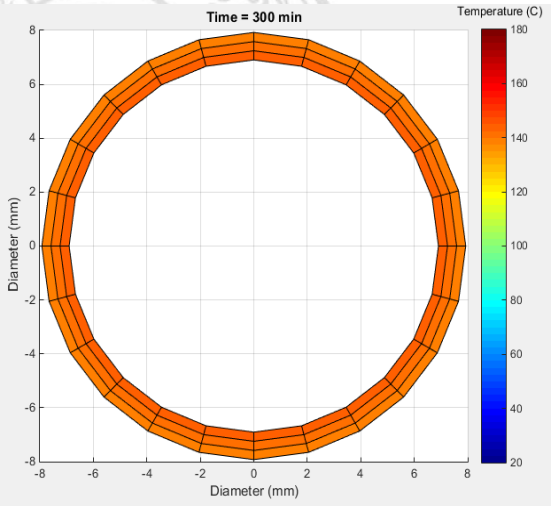

(d) Temperature distribution at 1:00 p.m.

Figure 6.10 Temperature distribution of evaporator section for clear sky day condition on October 14, 2016

The temperature distribution of evaporator section of clear sky day condition on October 14, 2016 and the cross-sectional view is presented in Figure 6.10. In Figure 6.7 (b) and Figure 6.10, it can be seen that the temperature has continuously been increased during 10:00 a.m. to 12:00 p.m. as shown in Figure 6.7 (b). It will affect to the temperature distribution to be increased as shown in Figure 6.10 (a) to Figure 6.10 (c). After that, the temperature distribution in Figure 6.10 (d) is decreased which a similar to Figure 6.7 (b) during 12:00 p.m. to 1:00 p.m.

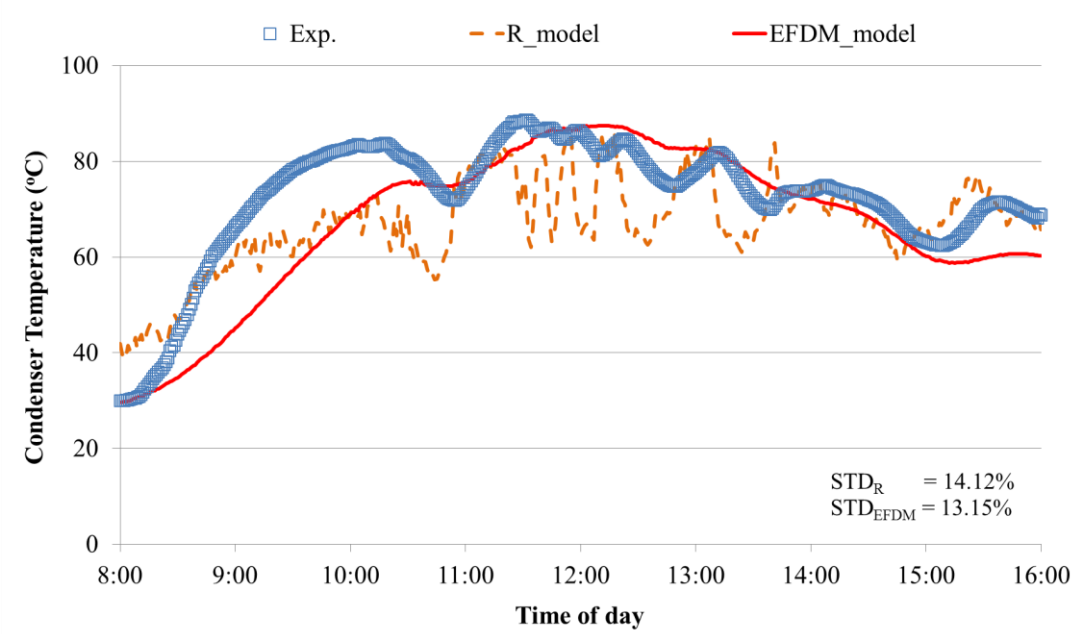

(a) Partly cloudy day condition (August 18, 2016)

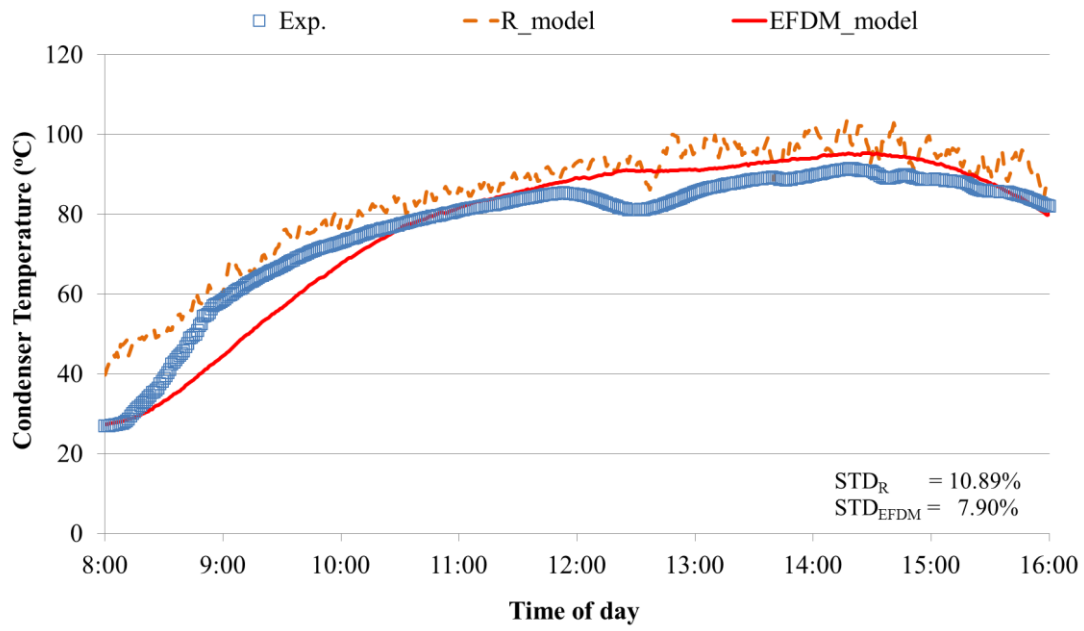

(b) Clear sky day condition (October 14, 2016)

Figure 6.11 Temperature of the condenser along with local time

From the mathematical models result, the standard deviation of the evaporator temperature on a partly cloudy day is ±14.27% for the thermal resistance method and ±12.93% for EFMD. On a clear sky day, the evaporator temperature's fluctuation of the

thermal resistance method is decreased due to smooth solar intensity. Therefore, the standard deviation of the thermal resistance method is ±15.84% on a clear sky day and ±11.05% for EFMD.

The variation of condenser temperatures is shown in Figure 6.11. It can be seen that temperatures of the mathematical models are the same trend with the experiment of both weather conditions. Moreover, temperature of the thermal resistance method on a partly cloudy day fluctuates more than EFDM. In Figure 6.11 (a), the condenser temperature of the experiment is gradually increased until reaches 10:00 a.m. local time which is the same time when both models are gradually increased until the local time reaches 11:00 a.m. for the thermal resistance method and 12:00 p.m. for EFDM. After that, the condenser temperature fluctuates along with local time. For a clear sky day in Figure 6.11 (b), the condenser temperature of the experiment and both models is slightly increased until the local time reaches 2:30 p.m. It also shows the maximum temperatures which are 90.67^{o}C for the experiment, 95.07^{o}C for the thermal resistance method, and 94.64^{o}C for EFDM. Then, the condenser temperature of the experiment and both models is slightly decreased to the final time at 4:00 p.m. The STD on a partly cloudy day is ±14.12% for the thermal resistance method and ±13.15% for EFDM. On a clear sky day, the STD of both models of thermal resistance method and EFDM are ±10.89% and ±7.90%, respectively.

The temperature distribution of condenser section is presented in Figure 6.12 for partly cloudy day condition on August 18, 2016 and Figure 6.13 represents clear sky day condition on October 14, 2016. It can be seen that the temperature distribution of condenser section of partly cloudy day condition is increased during 10:00 a.m. to 12:00 p.m. and then it is slightly decreased until the local time reaches 1:00 p.m. On the other hand, the temperature distribution of condenser section of clear sky day condition is increased during 10:00 a.m. to 1:00 p.m. It can be concluded that both of temperature distribution of condenser section is in a similar trend with the condenser temperature as shown in Figure 6.11.

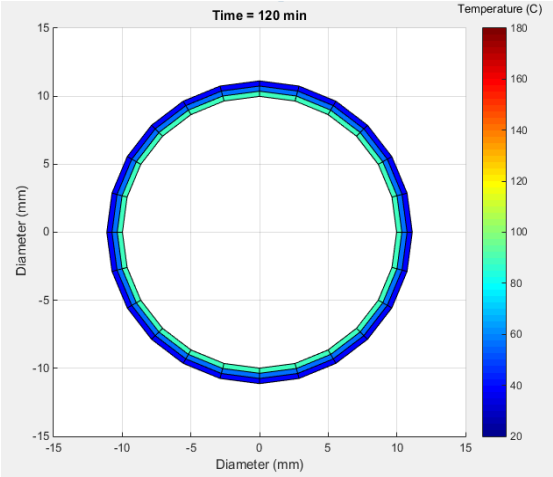

(a) Temperature distribution at 10:00 a.m.

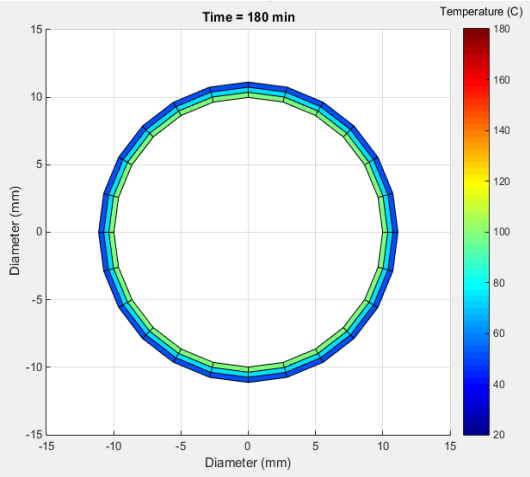

(b) Temperature distribution at 11:00 a.m.

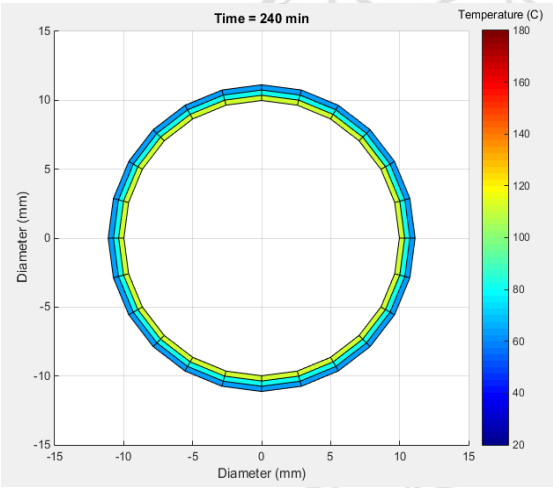

(c) Temperature distribution at 12:00 p.m.

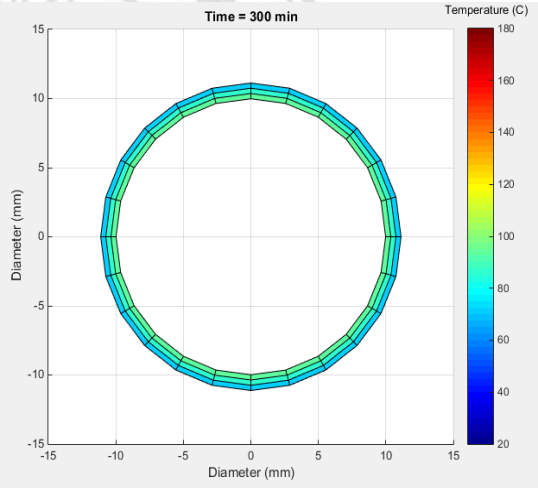

(d) Temperature distribution at 1:00 p.m.

Figure 6.12 Temperature distribution of condenser section for partly cloudy day condition on August 18, 2016

Temperature of hot water at the storage tank is presented in Figure 6.14. It is found that temperatures of the experiment and both models representing two different weather conditions are increased to the final time. However, in the early morning during 8:00 a.m. to 9:00 a.m., temperature of hot water is nearly constant because the solar intensity goes lower. Thereafter, the solar intensity is increased while temperature of hot water is gradually increased at 4:00 p.m. It can be concluded that the maximum temperature of hot water of both weather conditions is occurred in the early evening period around 4:00 p.m. For a partly cloudy day condition, the maximum temperatures of hot water are 52.45^{o}C, 58.00^{o}C, and 55.04^{o}C for the experiment, the thermal resistance method, and

the EFDM. The STD is ±11.05% for the thermal resistance method and ±5.11% for EFDM. Moreover, for a clear sky day condition, the maximum temperatures of hot water are 65.25^{o}C for the experiment, 75.85^{o}C for the thermal resistance method, and 71.66^{o}C for EFDM. The STD is ±11.63% for the thermal resistance method and ±7.33% for EFDM.

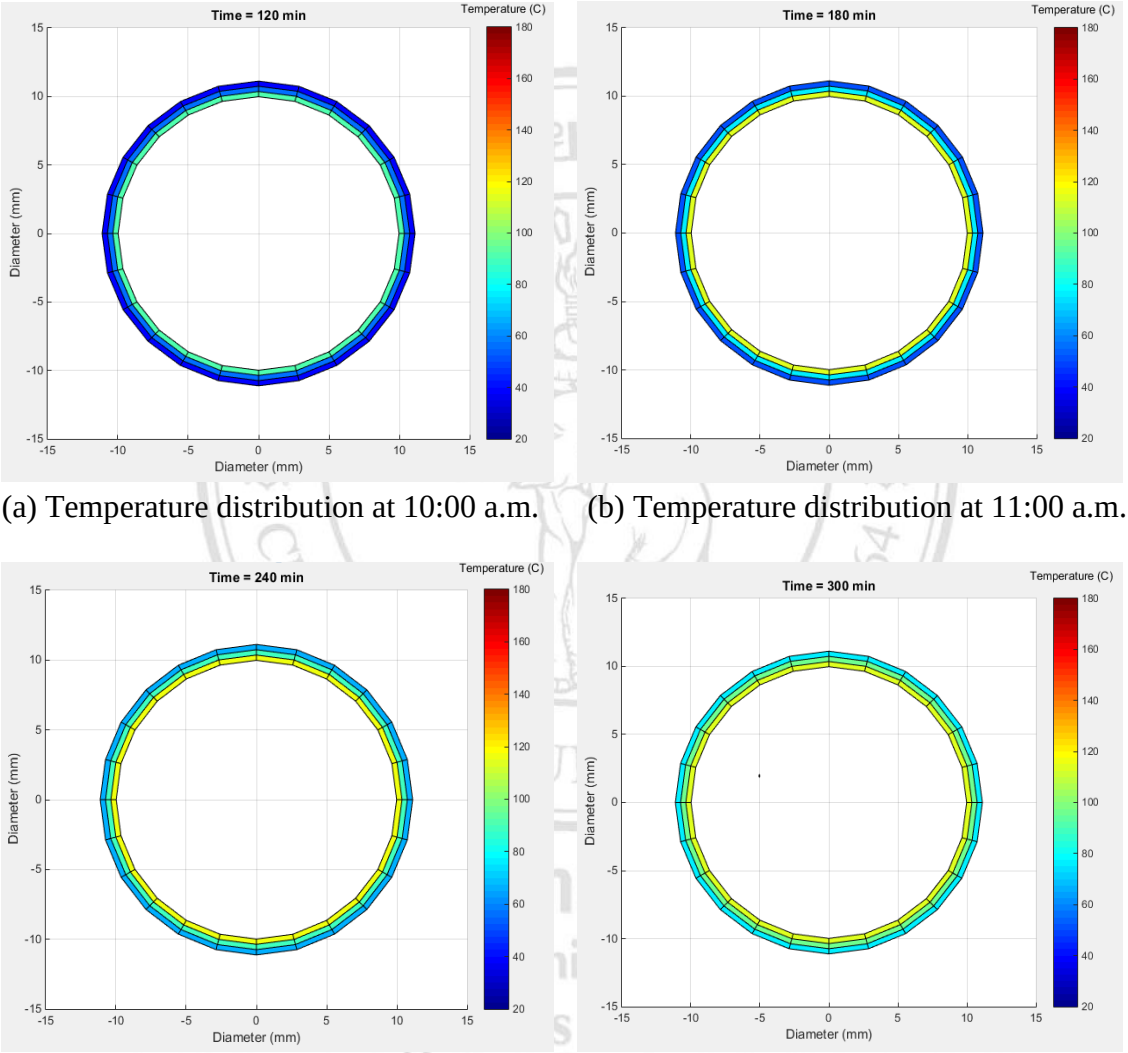

(a) Temperature distribution at 10:00 a.m. (b) Temperature distribution at 11:00 a.m.

(c) Temperature distribution at 12:00 p.m. (d) Temperature distribution at 1:00 p.m.

Figure 6.13 Temperature distribution of condenser section for clear sky day condition on October 14, 2016

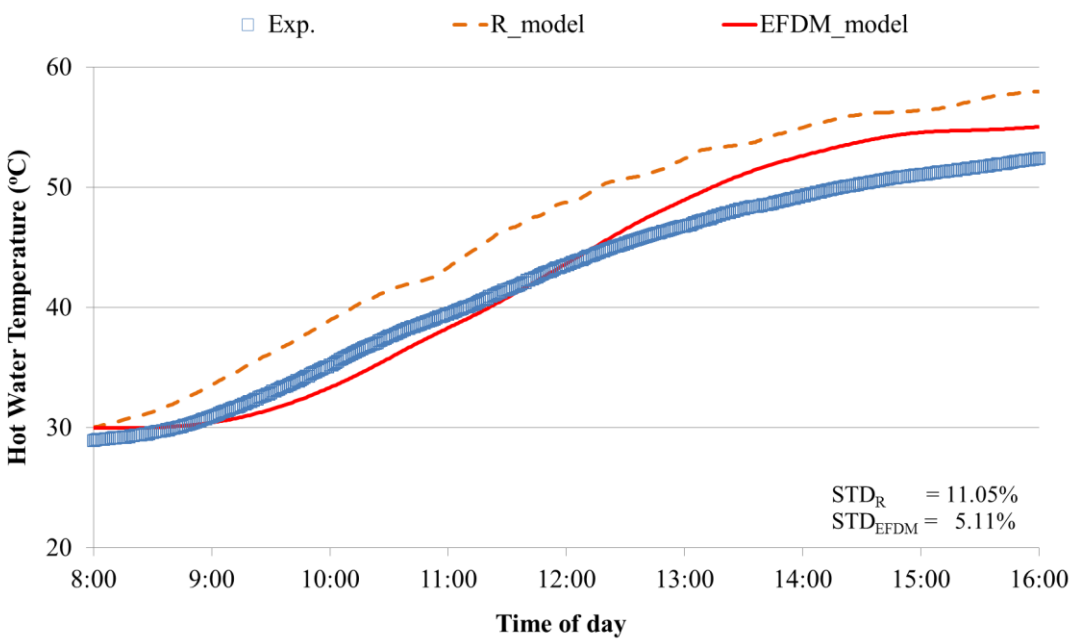

(a) Partly cloudy day condition (August 18, 2016)

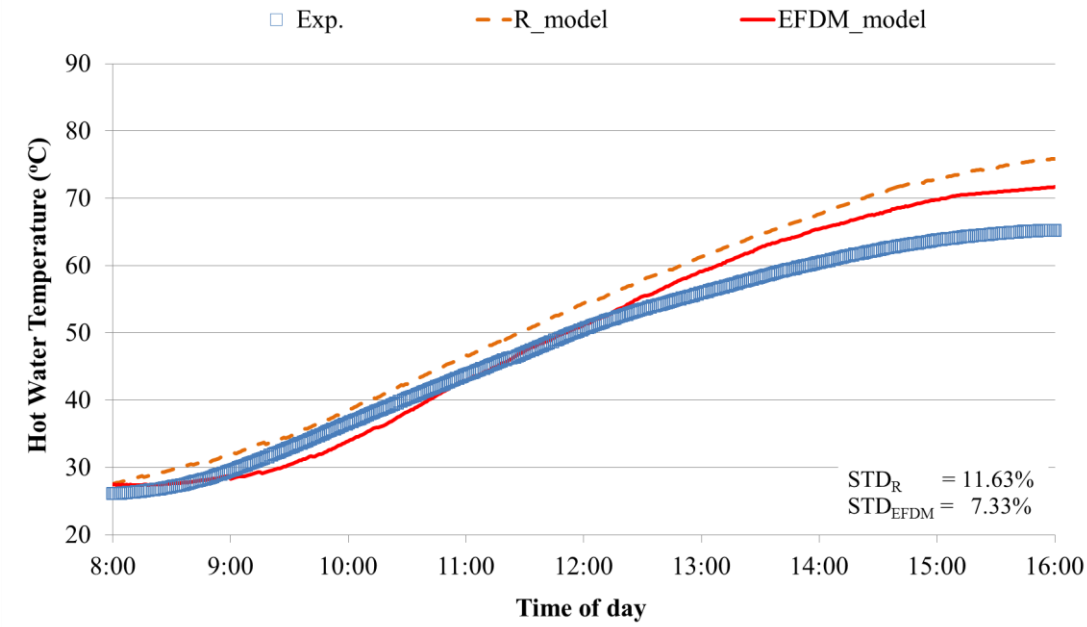

(b) Clear sky day condition (October 14, 2016)

Figure 6.14 Variation of water temperatures along with local time

Hot water temperatures of the mathematical models representing of both weather conditions are higher than the experiment because the mathematical model is negligible heat loss of the water pipe between the manifold and storage tank. Moreover, heat loss

of the experiment is higher after increasing the temperature of hot water. The relative error of hot water temperature of a partly cloudy day condition is about 9.56% of the thermal resistance method and 4.70% of EFDM. For a clear sky day condition, the relative error is about 13.44% of the thermal resistance method and 9.84% of EFDM.

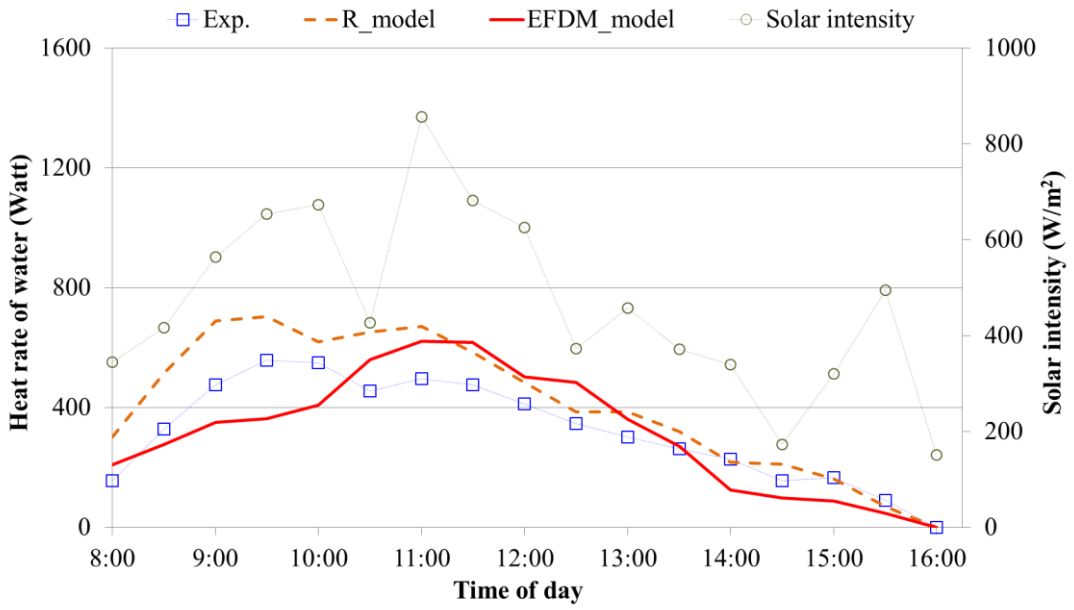

(a) Partly cloudy day condition (August 18, 2016)

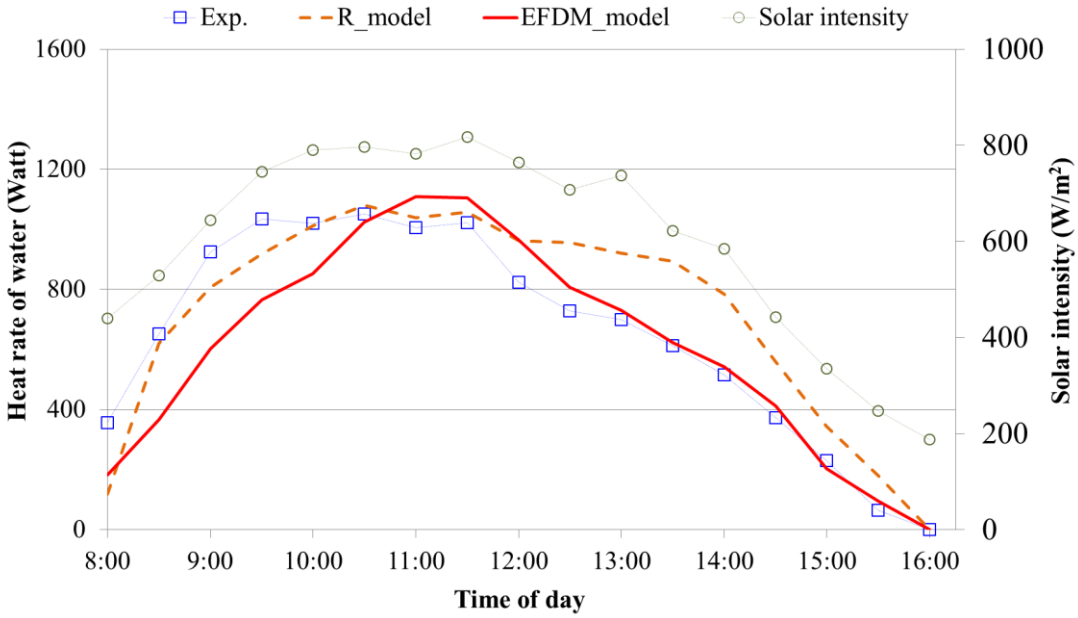

(b) Clear sky day condition (October 14, 2016)

Figure 6.15 Variation of the water heat rate along with local time

In order to analyze thermal efficiency of evacuated tube solar water heater system and water heat rate, it can be done by calculating the average of hot water temperature in every 30 minute. Accordingly, water heat rate of two weather conditions along with local time is presented in Figure 6.15.

From Figure 6.15, it should be noted that water heat rate always goes directly to the proportion of the solar incident on the collector system. For a clear sky day condition showing in Figure 6.15 (b), the water's maximum heat transfer rate of solar water heater system occurs at 10:30 a.m. which are 1,050.18 W for the experiment and 1,079.66 W for EFDM. However, for the thermal resistance method, the water's maximum heat transfer rate occurs at 11:00 a.m. in 1,109.86 W. For a partly cloudy day condition, the water's maximum heat transfer rate of the experiment and the thermal resistance occur at 9:30 a.m. which are 557.33 W and 702.66 W, respectively. Furthermore, the water's maximum heat transfer rate of EFDM is obtained about 621.89 W at 11:00 a.m. Then, heat rate of water of the experiment and both models is decreased to the final time.

The comparison of the deviation of the water heat rate between both models and the experimental results is shown in Figure 6.16. It is found that, the standard deviation between the experimental result and the mathematical models result on a partly cloudy day condition are 34.07% for the thermal resistance method and 29.38% for EFDM. For a clear sky day condition, there are 22.64% for the thermal resistance method and 21.10% for EFDM. From the mathematical models results, for a partly cloudy day, it is found that the solar radiation that has fluctuated will affect the deviations and it is higher than a clear sky day.

The thermal efficiency of the solar water heater systems of the experiment and the mathematical models are analyzed based on the local time from 8:00 a.m. to 4:00 p.m. for a partly cloudy day condition and a clear sky day condition as shown in Figure 6.17. It can be seen that the thermal efficiency on a partly cloudy day in Figure 6.17 (a) fluctuates and thermal efficiency highest are 46.46% for the experiment, 66.62% for the thermal resistance method, and 57.13% for EFDM at 10:30 a.m. On a clear sky day, the thermal efficiency of the experiment is suddenly increased from 35.36% to 61.70% and show the maximum value occurred at 9:00 a.m. For the thermal resistance is suddenly increased from 11.70% to 58.95% and show the maximum value occurred at 10:30 a.m.

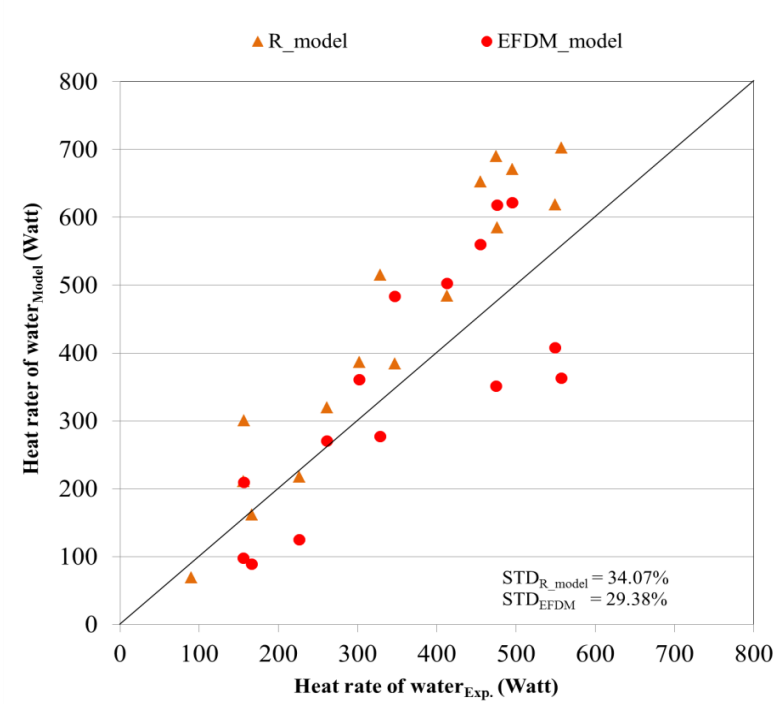

(a) Partly cloudy day condition (August 18, 2016)

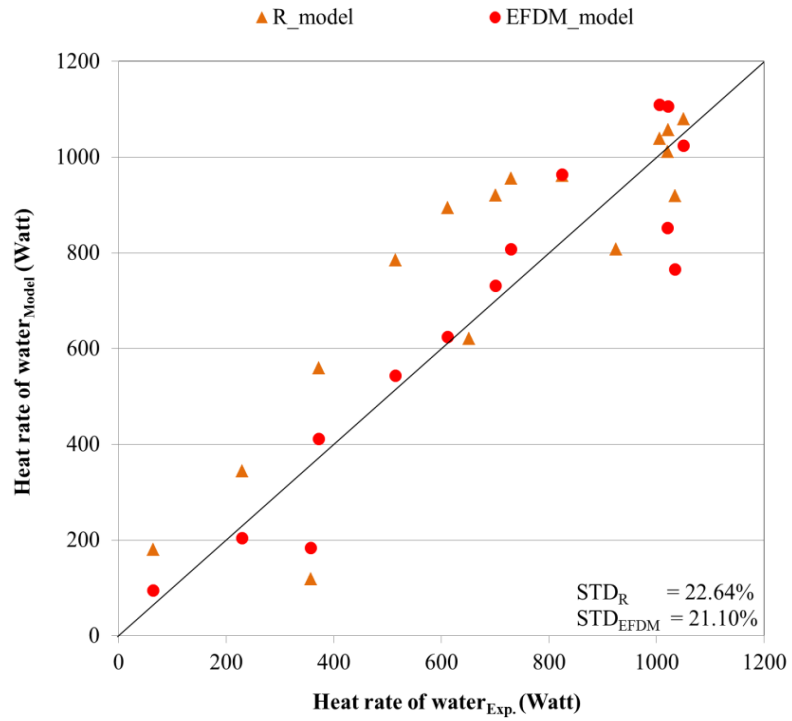

(b) Clear sky day condition (October 14, 2016)

Figure 6.16 Water heat rate compared to the experiment and mathematical models

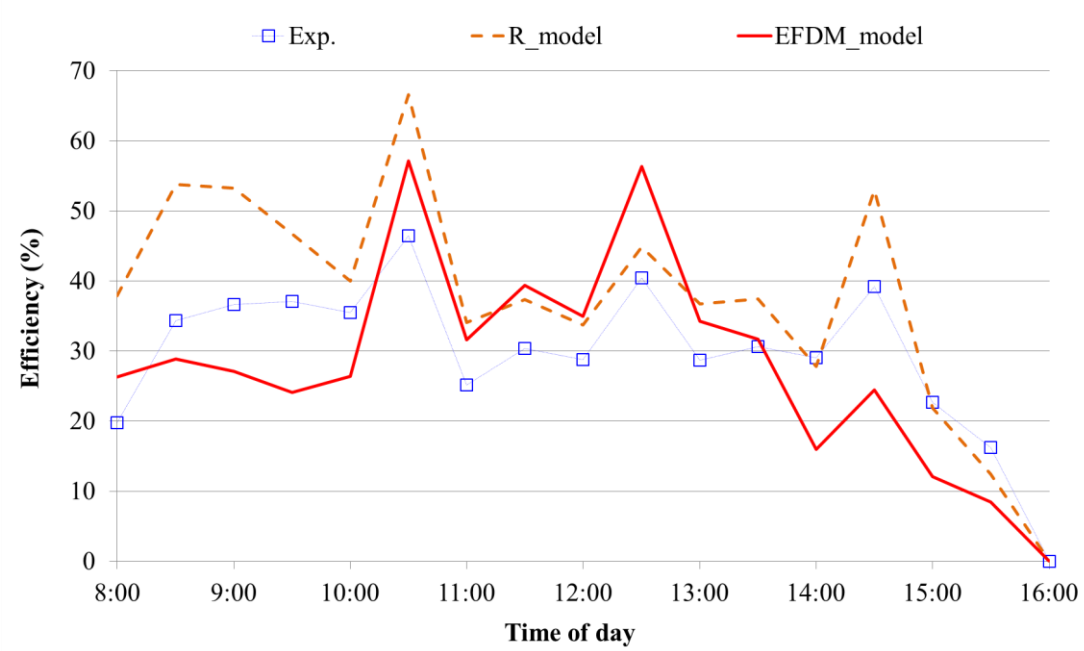

(a) Partly cloudy day condition (August 18, 2016)

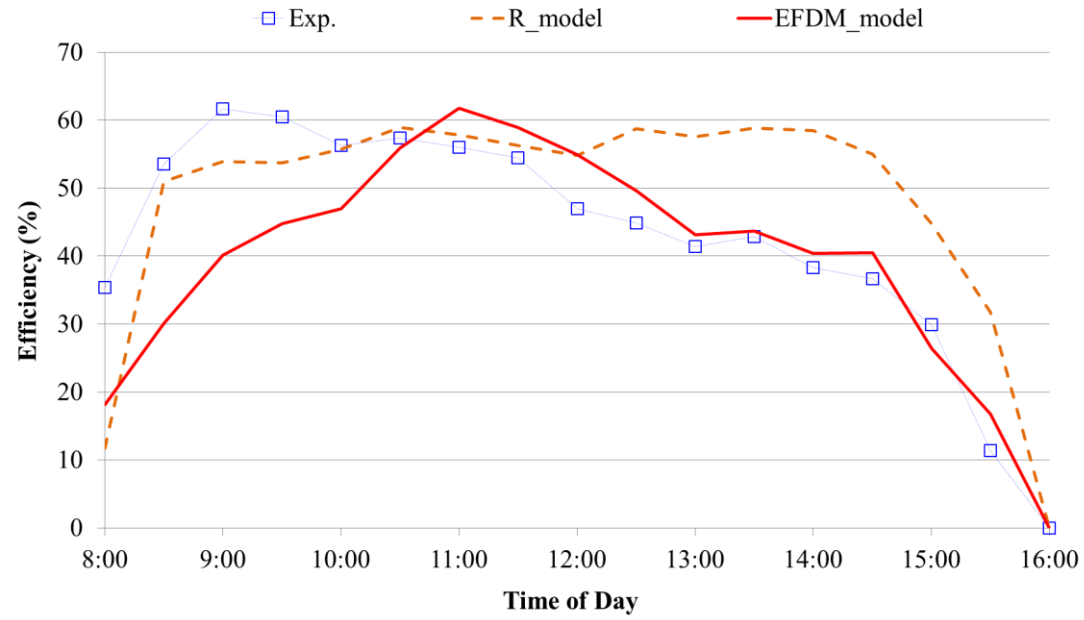

(b) Clear sky day condition (October 14, 2016)

Figure 6.17 Variation of the thermal efficiency compared to the experiment and mathematical models

While the EFDM result, the thermal efficiency is gradually increased from 18.15% to 61.76% and the maximum thermal efficiency occurs at 11:00 a.m. for 61.76%. The STD

of thermal efficiency is ±34.55% and ±30.16% for the thermal resistance method and EFDM on a partly cloudy day. The STD of a clear sky day, however, the thermal efficiency is ±27.79% and ±22.29% for the thermal resistance method and EFDM, respectively.

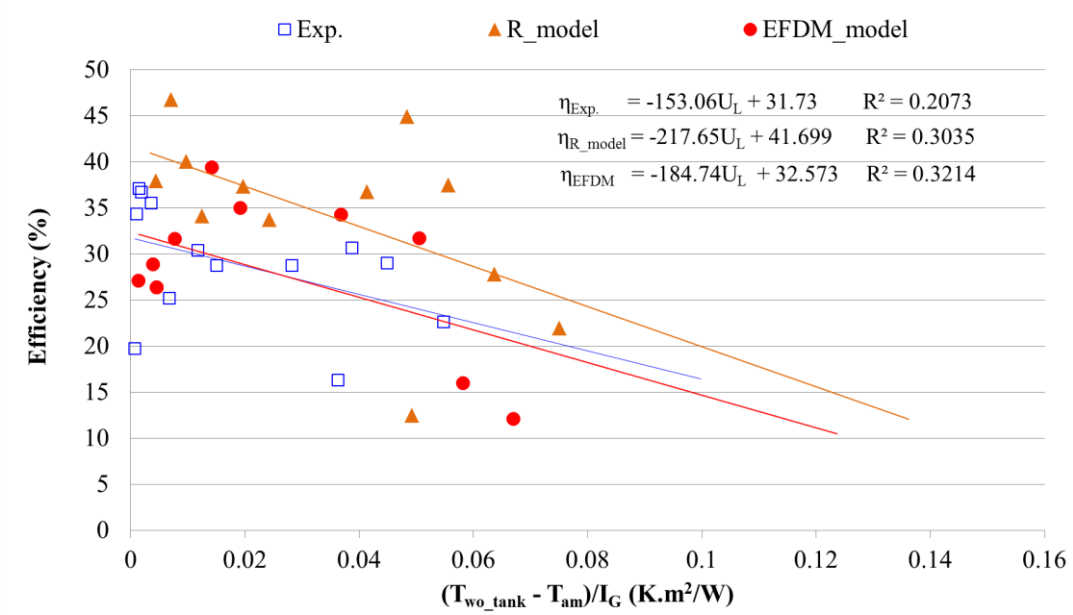

(a) Partly cloudy day condition (August 18, 2016)

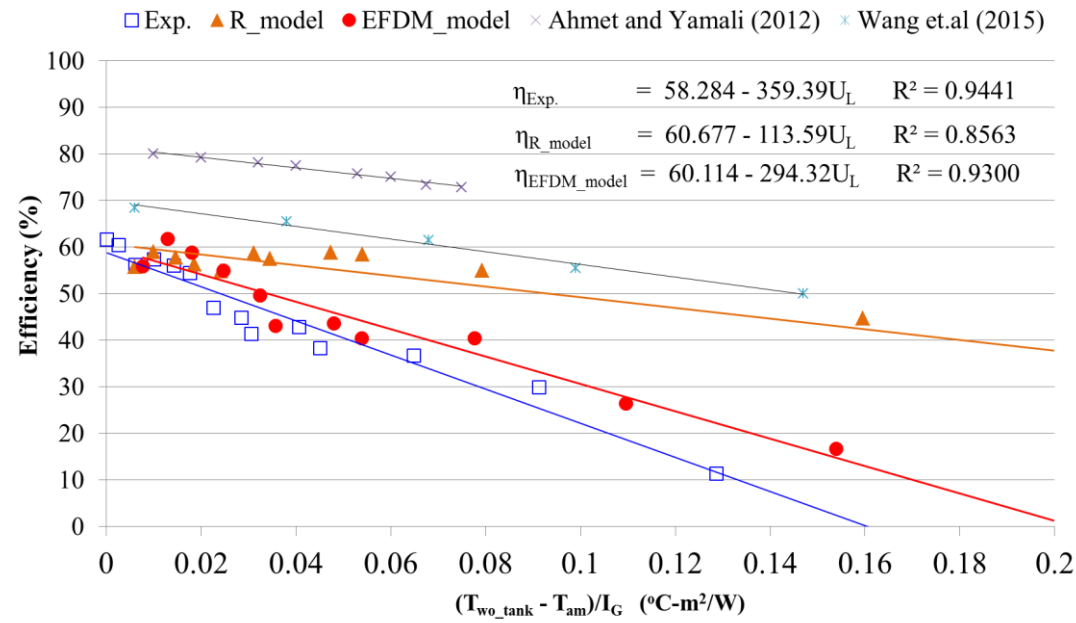

(b) Clear sky day condition (October 14, 2016)

Figure 6.18 Correlation of thermal efficiency and $(T_{wo\_tank} - T_{am})/I_G$

Thermal efficiency as a function of the environment is shown in Figure 6.18 and as functional conditions of $(T_{wo\_tank} - T_{am})/I_G$. In Figure 6.18, x-axis represents $(T_{wo\_tank} - T_{am})/I_G$ and y-axis represent the thermal efficiency. The results of regression analysis show that the equation of the experiment efficiency and the mathematical model efficiency are a linear function.

As shown in Figure 6.18 (b), the thermal efficiency of the presented results is in accordance well with Caglar and Yamali (2012) and Wang et.al (2015) which the results have a higher slope than the work of Caglar and Yamali (2012) and Wang et.al (2015). It should be noted that the slope of the thermal efficiency represents heat losses from the solar water heater system. Also, the thermal efficiency of the presented results is lower than that of Caglar and Yamali (2012) and Wang et.al (2015). The thermal efficiency of the experiment is 58.28%, which is about 3.14% lower than the EFDM model at 60.11% and lower than the thermal resistance method about 4.14% at 60.67%. An overall heat transfer coefficients of the system are 359.39 W/m^2-K for the experiment, 113.59 W/m^2-K for the thermal resistance method, and 294.32 W/m^2-K for EFDM.

According to Figure 6.18, it is found that the standard deviations on a partly cloudy day condition are higher than a clear sky day and a coefficient of determination (R-square) is less than a clear sky day. However, even on cloudy and clear sky day, the mathematical models show a good agreement with temperature prediction of the solar water heater and thermal efficiency compared to the experiment.

An uncertainty analysis is based on the method explained by Holman (1989). The measured variables in this study are temperature, solar intensity, and wind velocity. The calculated total uncertainty values are ±5.50% for water heat rate and ±5.85% for thermal efficiency.

6.2 Economics Analysis

For the economics analysis, the experiment result on October 14, 2016 is used for calculating the water heat rate by converting the heat energy compared to the electricity consumption of electric hot water heater. The conditions for economic analysis are assumed in Table 6.1, whereas the expenditure is shown in Table 6.2.

6.2.1 Simple Payback Period (SPP)

Simple Payback Period (SPP) is considered for the evacuated tube solar water heater system. It can be said that the result of payback period should be short because it will be used as a basis investment, which is the best choice for investment. Simple Payback Period is calculated by power consumption of electric water heater that produces hot water at 65^{o}C. For the operation of electric water heater, 6.8 hours of the electric consumption for 1 kWh as shown in Appendix D. Then, calculate the electric cost for producing hot water when considered electric rates is equal to 3.35 Baht/kWh, referred to Provincial Electricity Authority of Thailand.

Table 6.1 Conditions for economics analysis

Detail	Value
Yearly maintenance cost	10% of investment cost per year
Residual value	15% of investment cost per year
System life	10 years
Interest rate	6.5% (Government Savings Bank, 2016)

Table 6.2 Expenses of the evacuated tube solar water heater system and the electric water heater

Investment costs	Solar water heater	Electric water heater
Evacuated glass tube[1]	6,400	-
Copper tube[1]	7,820	-
Surcharge for construction and engineering[1]	4,520	-
Working fluid[1]	1,500	-
Miscellaneous[1]	3,000	-
Total investment costs (Baht)	23,240	12,700[2]

Remark: [1] Market cost, [2] Excerpted from http://www.e-sarnbestbuy.com

With daily total electric consumption producing hot water is about 6.8 hours at 1 kWh, the electric water heater uses the electricity for 2,482 kWh/years. The annual electrical consumption of electric water heater is 8,314.70 Baht/years as shown in Appendix E. On the other hand, yearly maintenance cost of the solar water heater

system is about 10% of investment cost as shown in Table 6.1 which is equal to 2,324 Baht/year. Therefore, the net cash inflow per year can be calculated by the annual electrical consumption deducted with yearly maintenance cost. It can be concluded that the simple payback period of the evacuated tube solar water heater system is 3 years 11 months.

6.2.2 Net Present Value (NPV)

Net Present Value (NPV) is considered to determine the present value of an investment by the discounted sum of all cash flows received from the solar water heater system, presented in Equation (2.59).

Data in Table 6.1 is used to calculate the net present value. From the results, it can be concluded that the net present value is positive at 23,312.13 Baht which indicates the solar water heater system earnings generated by investment exceed the anticipated costs. This concept is the basis for the net present value explained that the investments should be made with positive net present value.

6.2.3 Internal Rate of Return (IRR)

IRR measures the profitability of potential investments. For this reason, an internal rate of return is a discount rate that makes the NPV of all cash flows from a solar water heater equal to zero. To calculate IRR, NPV will be set in previous section equal to zero and solve for the discount rate, which is the IRR.

From the result in Appendix E, in this study, IRR is calculated at 22.35%. It means that the IRR has higher than the interest rate of investment cash flow. Therefore, the evacuated tube solar water heater will be practicality for the investments.

6.3 Conclusions

The mathematical models of evacuated tube solar water heater system with thermosyphon are validated accurate by the experiment results. The conclusions are as followings:

1) The thermal efficiency of the experimental result is 58.28%, which is about 3.04% lower than the EFDM model at 60.11% and lower than the thermal

resistance method is about 3.24% at 60.67%. An overall heat transfer coefficients of the system are 359.39 W/m^2-K for the experiment, 113.59 W/m^2-K for the thermal resistance method, and 294.32 W/m^2-K for EFDM. The standard deviations on a partly cloudy day condition are higher than a clear sky day and a coefficient of determination is less than a clear sky day. Moreover, even on cloudy and clear sky day, the temperature prediction and the thermal efficiency of mathematical models are show in good agreement with of the experimental results.

2) Temperatures of hot water at the storage tank are gradually increased until the local time reaches 4:00 p.m. The maximum temperature of hot water of two weather conditions is occurred in the early evening period around 4:00 p.m. For a partly cloudy day condition, the maximum temperatures of hot water are 52.45^oC, 58.00^oC, and 55.04^oC for the experiment, the thermal resistance method, and the EFDM, respectively. Conversely, for a clear sky day condition, the maximum temperatures of hot water are 65.25^oC for the experiment, 75.58^oC for the thermal resistance method, and 71.66^oC for EFDM.
3) For the mathematical model, the EFDM model is shown more accurate than the thermal resistance method about 1.00% for thermal efficiency and 6.05% for water temperature at the storage tank. It can be said that the thermal resistance method can be calculated faster than the EFDM.
4) For the economics analysis, the simple payback period of the evacuated tube solar water heater system is 3 years 11 months and the annual electrical consumption saving is 5,990.70 Baht/years.
5) Net Present Value (NPV) is positive at 23,312.13 Baht which indicates the solar water heater system earnings generated by investment exceed the anticipated costs. NPV will be set in previous section equal to zero and solve for the discount rate, which is calculated at 22.35%.